MINISTRY OF EDUCATION AND TRAINING
VIETNAM ACADEMY OF SCIENCE AND TECHNOLOGY

GRADUATE UNIVERSITY OF SCIENCE AND TECHNOLOGY

Pham Duy Tan

RESEARCH ON FABRICATION OF METAMATERIALS APPLIED IN NDIR SENSORS FOR CO_2 GAS DETECTION

SUMMARY OF DOCTORAL DISSERTATION IN MATERIALS SCIENCE

Major: Electronic Materials

Code: 9 44 01 23

Ha Noi - 2026

The dissertation is completed at: Graduate University of Science and Technology, Vietnam Academy of Science and Technology

Supervisors:

1. Supervisor 1: *Assoc. Prof. Dr. Bui Xuan Khuyen, Institute of Materials Science, Vietnam Academy of Science and Technology*
2. Supervisor 2: *Dr. Ho Truong Giang, Institute of Materials Science, Vietnam Academy of Science and Technology*

Referee 1: Assoc. Prof. Dr. Ngo Quang Minh, University of Science and Technology of Hanoi, Vietnam Academy of Science and Technology.
Referee 2: Assoc. Prof. Dr. Nguyen Thi Hoa, University of Transport and Communications, Ministry of Education and Training
Referee 3: Assoc. Prof. Dr. Nguyen Thi Hien, Thai Nguyen University of Sciences, Thai Nguyen University, Ministry of Education and Training

The dissertation is examined by Examination Board of Graduate University of Science and Technology, Vietnam Academy of Science and Technology at 2:00 PM, Friday, January 30, 2026.

The dissertation can be found at:
1. Library of the Graduate University of Science and Technology
2. National Library of Vietnam

INTRODUCTION

1. Necessity of the Dissertation

In the context of increasing climate change, monitoring air quality and agricultural emissions plays a crucial role in sustainable development and public health protection. In developing countries such as Vietnam, the monitoring systems for agricultural gas emissions and microclimate remain limited due to high costs and a lack of compact, high-precision sensors—particularly for CO_2 detection

For CO_2, its role in agriculture is highly diverse:

CO_2 serves as a raw material for photosynthesis, and an optimal concentration (800–1000 ppm) can increase vegetable yields by 20–40% [Wageningen]. It affects the growth of fungi and soil microorganisms and is also the main greenhouse gas (accounting for 76% of agricultural emissions according to FAO, 2021). The release of CO_2 from eroded soil reduces fertility and contributes to climate change.

Challenges of existing gas sensors: current gas sensors can be classified into two main groups:

- Chemical sensors (electrochemical, MOS, PID): low-cost but suffer from high drift, short lifespan, and poor selectivity.
- Physical sensors (UV, NDIR): more durable and selective, but expensive and bulky.

NDIR (Non-Dispersive Infrared) sensors operate based on the characteristic infrared absorption of gases (Figure 1), offering high selectivity and reliability. However, traditional NDIR systems rely on broadband sources and optical filters, leading to energy inefficiency and limited sensitivity at low concentrations. Increasing the source intensity or optical path length enlarges the system size and cost.

Solution from Metamaterials (MMs):

Metamaterials are artificially engineered structures with sub-wavelength periodicity, enabling unprecedented control over electromagnetic waves. In gas sensing, MMs can be integrated to:

- Replace traditional optical filters with highly selective metasurfaces;

- Create narrowband micro-thermal emitters through perfect absorption (MPA) and thermal emission at desired wavelengths;
- Enhance optical efficiency and miniaturize sensors, suitable for IoT and smart agriculture applications.

In Vietnam, pioneering work in this field has been conducted by Prof. Dr. Vu Dinh Lam's research group at GUST, Vietnam Academy of Science and Technology (VAST). The group has published numerous high-impact international papers on metamaterials and serves as a core team advancing this research direction in Vietnam. Related studies on metamaterials are also expanding at other institutions, including Assoc. Prof. Dr. Tran Manh Cuong (Hanoi National University of Education), Assoc. Prof. Dr. Vu Van Yem (Hanoi University of Science and Technology), Assoc. Prof. Dr. Nguyen Thi Hien (Thai Nguyen University), Dr. Le Van Quynh (VinUni), and Assoc. Prof. Dr. Nguyen Thi Quynh Hoa (Vinh University). Most of these works have focused on modeling and design, while practical applications for gas sensing remain limited.

2. Objectives and Contributions of the Dissertation

This dissertation aims to successfully fabricate metamaterial structures for application in advanced CO_2 gas sensors, with the following specific objectives:

- Clarify the interaction mechanism between metamaterials and infrared electromagnetic radiation;
- Perform simulations to determine metamaterial structures capable of selectively filtering infrared radiation at the characteristic absorption wavelength of CO_2 (4.26 μm);
- Experimentally fabricate metamaterial layers integrated into non-dispersive infrared (NDIR) CO_2 sensors.

Scientific and practical significance:

- Successfully simulated metamaterial structures operating in the infrared region for integration into NDIR sensors, including direct incorporation into micro-thermal emitters and reflective layers to generate narrowband infrared emission (around 4.26 μm) characteristic of CO_2 gas.

- Fabricated and experimentally tested metamaterial layers for use in reflective configurations within NDIR-type CO_2 gas sensors.

3. Structure of the Dissertation

Apart from the Introduction, Conclusion, and References, the dissertation consists of four chapters

- Chapter 1: Overview of metamaterials applied in gas sensors.
- Chapter 2: Research methodology for gas-sensor structures integrated with metamaterials.
- Chapter 3: Design and optimization of metamaterial structures for narrowband micro-thermal emitters.
- Chapter 4: Design and optimization of metamaterials for optical filters in gas sensors.

CHƯƠNG 1. OVERVIEW OF METAMATERIALS (MMs) APPLIED IN GAS SENSORS

1.1. Overview of Infrared Absorption Gas Sensors

1.1.1. Operating Principle of CO_2 Gas Sensors

The non-dispersive infrared (NDIR) gas sensing principle is based on the Lambert–Beer law:

$$I = I_0 e^{-\alpha l c} \quad (1.1)$$

where α is the absorption coefficient specific to CO_2 at the wavelength of 4.26 μm. This method offers high selectivity, a wide measurement range (from ppm to %vol), fast response time (a few seconds), and long operational lifetime. A typical NDIR sensor employs a dual-channel configuration (Figure 1.3): one measurement channel at 4.26 μm (sensitive to CO_2 absorption), and one reference channel at 3.9 μm (non-absorbing region). The CO_2 concentration is determined by the following expression:

$$c = -q \ln\left(\frac{U_1}{U_2}\right) \quad (1.5)$$

which eliminates the influence of source intensity fluctuations and environmental noise.

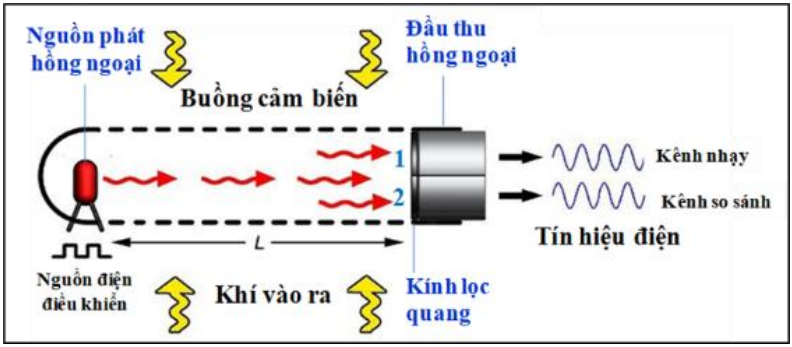

Figure 1.3. Schematic of a CO_2 gas sensor based on the NDIR principle with a dual-detector configuration.

1.1.2. Improvement Strategies for NDIR Gas Sensors

Conventional NDIR sensors are limited by their broadband infrared sources and optical filters, leading to energy loss and reduced efficiency.

Several enhancement strategies have been proposed:

- Increasing the source intensity → reduces emitter lifespan;
- Extending the optical path → increases system size;
- Using narrowband laser sources → improves performance but significantly raises cost

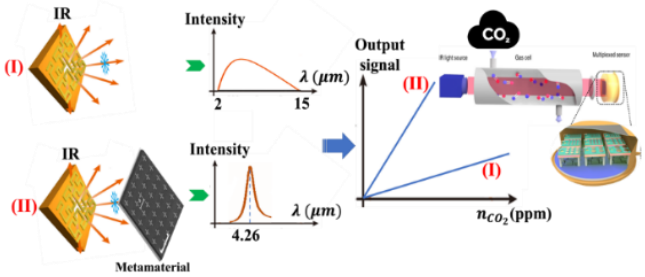

Figure 1.5. Illustration of metamaterial integration for the development of an advanced CO_2 gas sensor based on the infrared absorption principle.

A promising solution is to incorporate metamaterials into the system (Figure 1.5). MMs can convert broadband emission into narrowband radiation at the target wavelength, thereby improving efficiency, reducing size, and lowering power consumption.

1.2. Metamaterial Models Applied in NDIR Gas Sensors

1.2.1. Absorptive Metamaterials Integrated into Infrared Emitters

A Metamaterial Perfect Absorber (MPA) typically features a three-layer structure (metal–dielectric–metal), in which the top metallic layer consists of resonant patterns (e.g., cross-shaped elements) as shown in Figure 1.6(b). The MPA achieves nearly 100% absorption at the designed wavelength through resonant coupling and impedance matching.

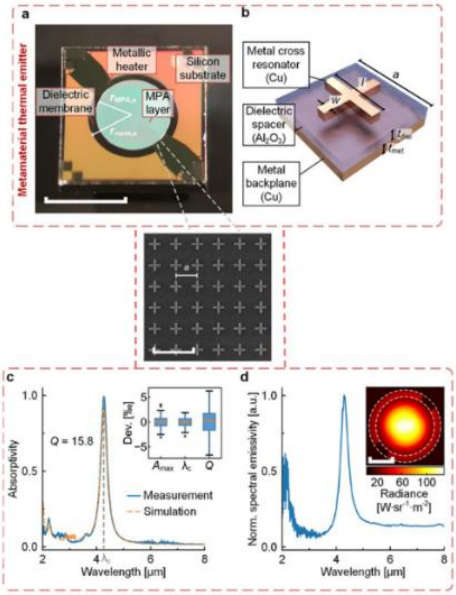

Figure 1.6. (a) Infrared emitter integrated with MMs; (b) Unit cell structure of the MM; (c) Simulated absorption spectrum of the MM; (d) Relative emission spectrum of the IR emitter integrated with the MM. The inset shows the corresponding thermal radiation image.

1.2.2. Transmissive Metamaterials Integrated into Infrared Emitters

Another approach involves the use of transmissive-type metamaterials to narrow the emission bandwidth, as proposed by Ruijia Xu et al. [47], yielding promising results. The device integrates a transmissive MM structure onto a micro-heater (Figure 1.7a). To achieve a narrower emission linewidth, the transmissive MMs are deposited directly on the micro-heater surface.

The radiation power of the IR emitter integrated with transmissive MMs under different DC bias voltages is shown in Figure 1.7(c).

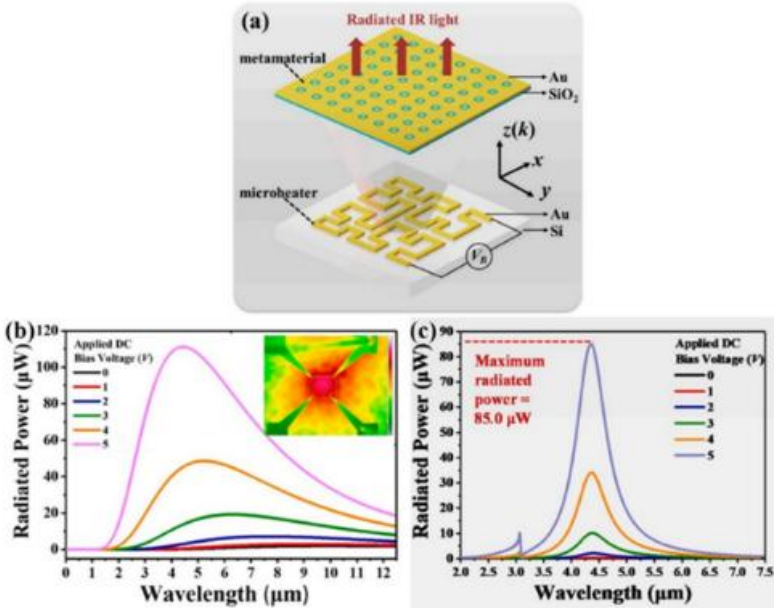

Figure 1.7. (a) Infrared emitter based on a micro-heater integrated with transmissive MMs; (b) Emission power of the micro-heater under different DC bias voltages (inset: thermal image recorded by an IR camera); (c) Emission power of the MM-integrated infrared emitter at various applied voltages.

1.3. Summary of Chapter 1

The integration of metamaterials into broadband infrared emitters to generate narrowband infrared radiation is a novel and rapidly emerging research direction worldwide. The design and simulation of MM structures enable the generation of infrared radiation at desired wavelengths, paving the way for advanced NDIR CO_2 gas sensors based on infrared absorption, as well as for broader applications in other spectral and technological fields. The MM layer can be integrated either directly on the emitter surface or placed at a specific distance from it. When broadband IR emission passes through the MM layer, the resulting output exhibits distinct, narrow spectral peaks corresponding to the designed resonant wavelengths.

CHAPTER 2. RESEARCH METHODS AND DESIGN OF NDIR SENSOR STRUCTURES BASED ON METAMATERIALS

2.1. Equivalent Circuit Modeling Using LC Resonance

This approach provides a simple and intuitive analytical tool to quickly predict the resonant frequency of a metamaterial structure based on its geometrical parameters and material properties. In this model, the electromagnetic behavior of MMs is represented by inductive (L) and capacitive (C) components.

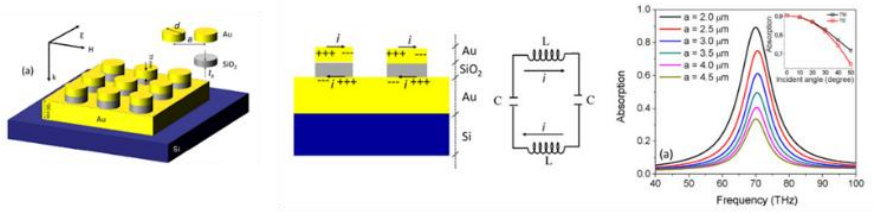

(a) (b) (c) (d)

Figure 2.1. Disk-shaped MM structure and its equivalent LC circuit model: (a) 3D structure of the MM; (b) Layered disk-shaped MM geometry; (c) Equivalent LC circuit at magnetic resonance frequency; (d) Equivalent LC circuit at electric resonance frequency

Basic principle: A metamaterial structure (e.g., a metallic disk pair) behaves as an RLC resonant circuit when excited by an incident electromagnetic wave. The magnetic resonance frequency (f_m) is determined by:

$$f = \frac{1}{2\pi\sqrt{LC}} = \frac{2}{\pi^2 d\sqrt{\alpha\epsilon\mu}} \quad (2.2)$$

2.2. Electromagnetic Simulation Method

Numerical modeling was performed using CST Microwave Studio and COMSOL Multiphysics, both based on the Finite Element Method (FEM) to solve Maxwell's equations. Design procedure: Constructing the Unit Cell: The MM unit cell (e.g., a three-layer metal–dielectric–metal structure with patterned top geometry) is modeled in CST to represent the basic repeating element. Applying Boundary Conditions: Periodic Boundary Conditions (PBCs) are imposed to simulate an infinitely periodic MM array,

closely approximating the physical material sample. Defining Excitation and Detection: A plane wave is normally incident on the MM surface, while detectors are placed to measure the scattering parameters (S_{11} and S_{21}), corresponding to reflection (R) and transmission (T). The absorption coefficient is then obtained as (A = 1 - R - T).

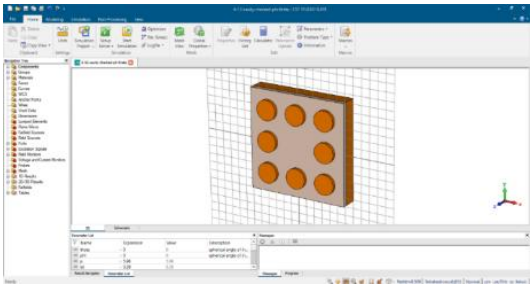

Figure 2.9. MM structure modeled in CST Microwave Studio for simulation of infrared absorption characteristics.

2.3. Design of NDIR Gas Sensors Integrated with Metamaterials (MMs)

2.3.1. NDIR Sensor with Transmissive MM Configuration

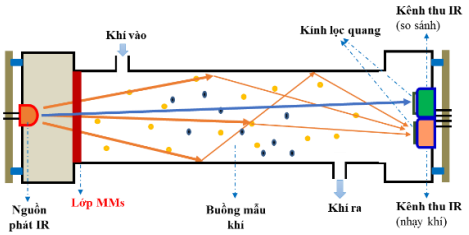

Figure 2.13. Configuration of an NDIR sensor integrated with transmissive MMs.

In this configuration, the metamaterial layer can be directly integrated onto the surface of the infrared (IR) emitter—typically a planar emitter. This approach allows the thermal energy and IR radiation generated by the emitter to be completely absorbed and re-emitted by the MM layer at distinct narrowband spectral peaks. Consequently, the IR source and the MM layer can be considered a unified narrowband IR emitter. However, such integration requires complex multilayer fabrication processes to obtain a fully functional emitter. A more flexible alternative is to place the MM layer

at a certain distance from the IR source, where it acts as an absorber and re-emitter, interacting with the broadband radiation to produce the desired spectral peaks. This sensor configuration is versatile and can be adapted to various types of IR emitters. In this dissertation, the research focuses primarily on simulation and structural design of MM layers to identify optimized configurations suitable for transmissive-type NDIR sensors.

2.3.2. NDIR Sensor with Reflective MM Configuration

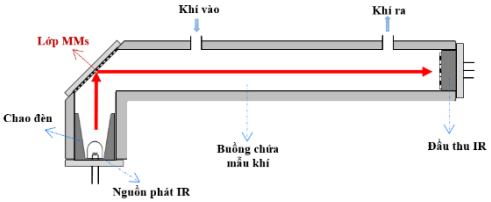

Figure 2.14. Configuration of an NDIR sensor integrated with reflective MMs.

This design introduces an improved approach in which a metamaterial layer is integrated to convert broadband infrared emission into narrowband radiation corresponding to the target gas absorption line (for CO_2, $\lambda = 4.26$ μm). Unlike conventional optical filters, which typically transmit only 70–80% of the target wavelength, the MM layer acts as a spectral converter rather than a mere filter. Specifically, the MM layer absorbs broadband IR radiation and re-emits it with strong intensity concentrated at the desired wavelengths. This behavior arises from electromagnetic coupling among the MM unit cells, combined with thermal absorption and re-emission processes. Such an approach can eliminate the need for traditional optical filters, thereby simplifying the sensor structure and reducing manufacturing costs.

2.4. Summary of Chapter 2

Both transmissive and reflective configurations of MM-based NDIR sensors were investigated. In the transmissive configuration, the MM layer serves as part of an advanced IR source capable of producing distinct emission peaks matched to CO_2 absorption features. In the reflective configuration, the dissertation proposes a design suitable for fabrication and experimental integration into an NDIR CO_2 gas sensor.

CHAPTER 3. DESIGN AND OPTIMIZATION OF METAMATERIAL STRUCTURES FOR NARROWBAND MICRO-THERMAL EMITTERS

3.1. Micro-Thermal Emitters Based on Multi-Resonant MPA Structures

3.1.1. Simulation and Design

Objective:

To design a Metamaterial Perfect Absorber (MPA) capable of achieving near-total absorption and subsequent narrowband thermal emission at the target wavelength of 4.26 µm.

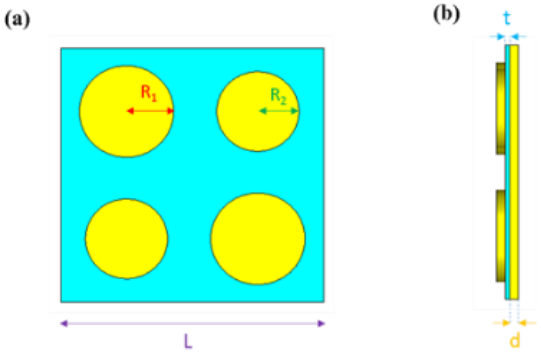

Figure 3.1. Unit cell of the designed MM: (a) top view; (b) side view.

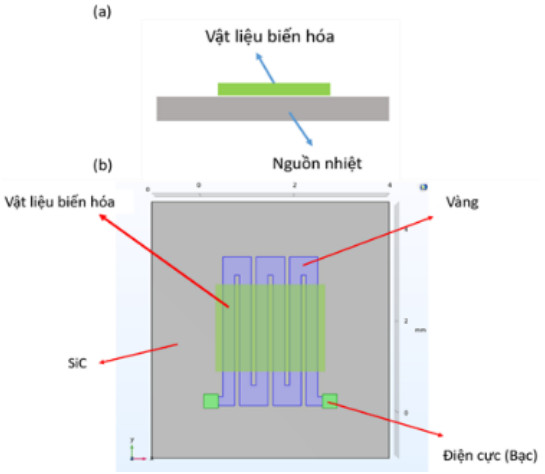

Figure 3.2. (a) General schematic of the MM-based thermal emitter; (b) top view of the MM emitter structure

3.1.2. Results and Discussion

The absorption spectrum of the MM structure (Figure 3.1) as a function of wavelength is shown in Figure 3.4.

The MM layer exhibits absorption peaks of 92% and 97% at wavelengths of 3.75 µm and 4.2 µm, respectively.

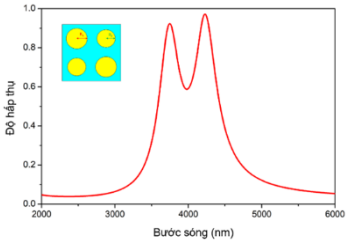

Figure 3.4. Absorption spectrum of the MM structure with coupled circular-disk resonators

These results indicate that the designed structure is highly suitable for NDIR gas sensing, as the spectral peaks coincide with the characteristic CO_2 absorption band.

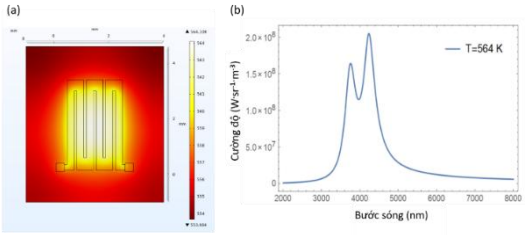

Figure 3.9. (a) Temperature distribution on the emitter surface at applied voltage U = 1.5 V; (b) Emission intensity of the MM layer at T = 564 K.

Simulation results show that when a voltage of 1.5 V is applied to the zigzag-pattern micro-heater, the surface temperature reaches 564 K.

The corresponding emission spectrum of the MM structure (Figure 3.9 b) exhibits two emission peaks at 3.7 µm and 4.2 µm, with intensities of approximately 1.6×10^8 and 2×10^8 $W \cdot sr^{-1} \cdot m^{-3}$, respectively, at the same input voltage.

The structure demonstrates practical feasibility owing to its polarization-independent response and angular stability—the absorption

remains around 70% even at an incidence angle of 60^0, confirming the robustness of the design.

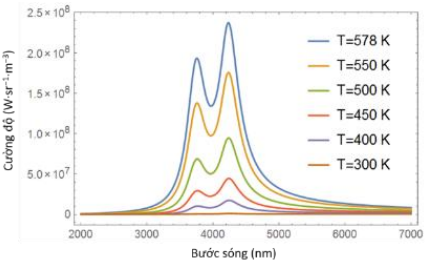

Figure 3.10. Emission intensity of the MM layer at various operating temperatures.

3.2. Micro-Thermal Emitter with Resonant-Cavity Structure

3.2.1. Design and Simulation of a Spiral Micro-Heater

A typical CO_2 infrared (IR) gas sensor based on the NDIR principle consists of four main components: (1) a broadband IR source (1–15 μm), (2) a detector, (3) an optical filter that transmits both the CO_2 absorption wavelength and a reference wavelength, and (4) a sample chamber. In our design, the micro-heater acts as the IR emitter integrated with the MM layer. The schematic of the device is shown in Figure 3.11(a). The design includes a silica substrate with a thickness of 0.2 mm and a radius of 3 mm. A gold spiral wire (thickness 50 nm, outer radius 1.5 mm) is patterned on the substrate and connected to silver electrodes at both ends. The MM layer is deposited on top of this structure.

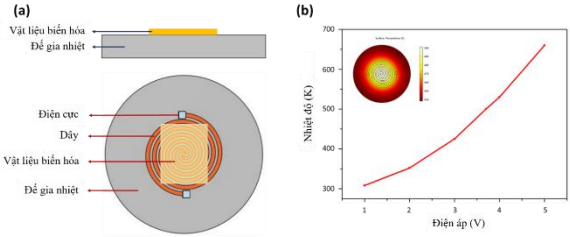

Figure 3.11. (a) Structure of the micro-heater integrated with the MM layer; (b) Relationship between the maximum surface temperature and applied voltage (inset: simulated temperature distribution on the micro-heater surface at 3.7 V).

At thermal equilibrium, the radiation intensity of the emitter can be described by the Stefan–Boltzmann law for a blackbody, which is derived from the Planck radiation law for an ideal emitter:

$$I_0(\lambda, T) = \frac{2hc^2}{\lambda^5} \frac{1}{e^{\left(\frac{hc}{\lambda k_B T}\right)} - 1} \quad (3.2)$$

where $I_0(\lambda,T)$) is the spectral radiance, h is Planck's constant, c is the speed of light in vacuum, λ is the wavelength, kB is Boltzmann's constant, and T is the absolute temperature (Kelvin).

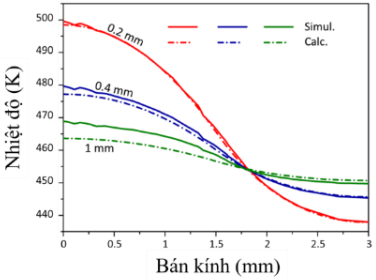

Figure 3.12. Surface temperature distribution along the radial direction for different substrate thicknesses.

3.2.2. Results and Discussion

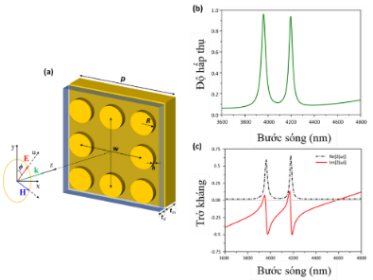

Figure 3.13. (a) MM structure comprising eight circular disks surrounding a cavity; (b) absorption spectrum; (c) impedance of the structure.

The structure consists of three layers: two gold layers separated by a polyimide dielectric of thickness t_d = 0,29 μm. Simulations use a polyimide relative permittivity of 3.5 and a dielectric loss tangent of 0.0027. The bottom layer is a continuous gold film with thickness t_m = 0,75 μm ; the top layer is patterned with eight circular disks. The optimized center-to-center spacing is

w = 3,68 μm. Each disk has thickness h = 0,19 μm, and radius R = 0,63 μm the unit-cell period is p = 5,96 μm. Figure 3.13(b) shows the absorption spectrum, exhibiting two absorption peaks at 3960 nm and 4197 nm with peak absorptances of 96.3% and 94.1%, respectively.

Figure 3.18 presents the emission spectra obtained from the MM-integrated micro-heater at different temperatures for θ=0. The results demonstrate a substantial suppression of unwanted out-of-band emission while maintaining strong intensity at the target wavelengths. Overall, the narrowband emission of the MM-integrated IR emitter enables low power consumption, which is advantageous for the development of spectrally tailored, potentially modulated IR sources in future work..

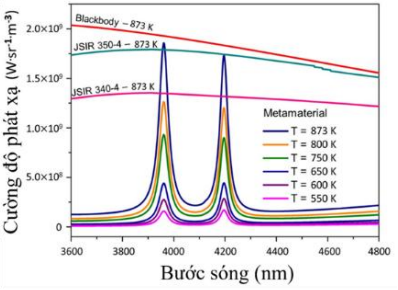

Figure 3.18. Emission spectra of the MM layer integrated with the micro-heater, compared to commercial IR sources, at various temperatures for θ = 0.

3.3. Energy-Efficient Optimization of the MPA Micro-Thermal Emitter

3.3.1. Design and Simulation

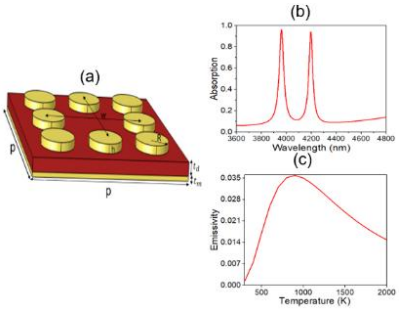

Figure 3.20. (a) Schematic of the proposed metamaterial structure; (b) absorption spectrum; (c) dependence of normalized emissivity on temperature.

Optimization targets not only high absorptance but also thermal compatibility and efficiency when integrated with a micro-heater. Figure 3.20(c) depicts the temperature dependence of the normalized emissivity. The proposed MMs exhibit promising characteristics for applications requiring selective IR emission while minimizing energy consumption. With normalized emissivity values ε ranging from 0.14% to 0.35% across different temperatures, the materials are engineered to emit specifically within the desired IR band, which is essential for precision IR detection. Such spectrally concentrated emission reduces wasted energy associated with unnecessary wavelengths, yielding higher energy efficiency than conventional blackbody-based thermal emitters. Moreover, concentrated emission contributes to longer operational lifetime for IR detection systems incorporating our MM technology.

3.3.2. Design of a Micro-Thermal Emitter Integrated with MMs

To mitigate radiative loss, a 50 nm gold layer is deposited on the back side of the polyimide substrate in the heated region (Figure 3.24a). Owing to its high reflectivity, gold effectively reflects thermal radiation back into the system, thereby reducing overall electrical power consumption. In addition, the MM is designed for efficient, spectrally selective emission, further lowering energy usage compared to ideal-blackbody-based thermal sources.

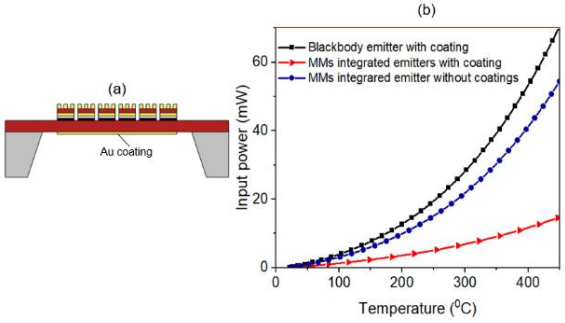

Figure 3.24. (a) Cross-sectional view of the emitter with Au back-coating; (b) Input power versus average temperature for different emitter types.

Figure 3.25(a) illustrates the surface temperature distribution of the coated MM-integrated emitter when the average temperature in the active region is 300^0C. The temperature is nearly uniform across the active area and drops rapidly to ambient at the membrane edge. A simplified model approximates the square membrane by an equivalent circular membrane (Figure 3.25b). The radius of the circle is chosen to minimize the non-overlapping area between the square and the circle; specifically, the radius is 0.5412, where a is the side length of the square.

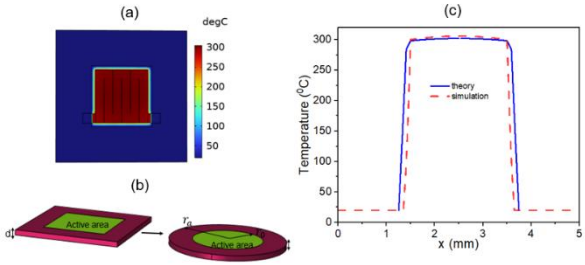

Figure 3.25. (a) Surface temperature distribution of coated emitters; (b) reduction to a one-dimensional heat-transfer model via circular approximation; (c) temperature distribution along the x-axis

We further performed a transient thermal analysis to evaluate the response time of the IR emitters, i.e., how quickly the emitter reaches steady-state temperature after a change in input power. As shown in Figure 3.26, a coated emitter subjected to an input power of 6.8 mW requires 1.65 s to reach a steady-state temperature of 300^0C

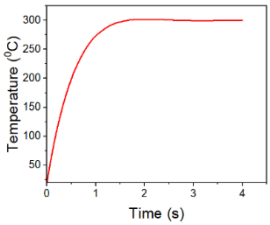

Figure 3.26. Temporal evolution of temperature.

3.4. Chapter 3 Summary

This chapter presented the detailed design and optimization of MPA-based structures to realize a high-performance, narrowband micro-thermal

emitter. Simulation results confirm the feasibility of producing quasi-monochromatic emission at 4.26 μm. The choice between multi-resonant and cavity-resonant architectures, together with thermal optimization, is a crucial step toward transitioning from simulation to practical fabrication of MM-integrated emitters, promising superior performance over conventional broadband sources.

CHAPTER 4. DESIGN AND OPTIMIZATION OF MMs FOR OPTICAL FILTERS IN GAS SENSORS

4.1. NDIR Sensor with Transmissive MM Configuration

4.1.1. Sensor Structure Design

Objective:

To develop a metamaterial-based optical filter that selectively transmits at the characteristic CO_2 absorption wavelength (4.26 μm) while reflecting other wavelengths, thereby replacing conventional optical filters.

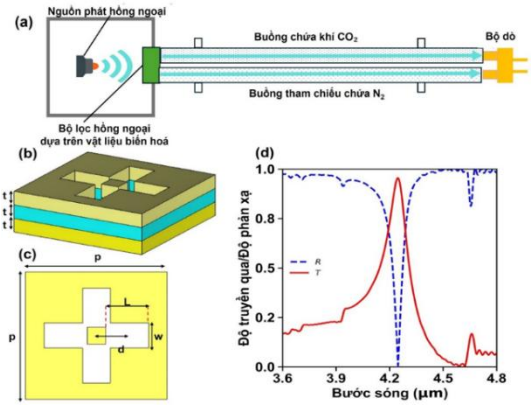

Figure 4.1. (a) Gas-sensor configuration; (b), (c) MM-based filter structure (3D view and top view); (d) transmission and reflection spectra.

Sensor configuration: A standard dual-channel NDIR system comprising: IR source → MM filter → gas sample chamber → thermopile detector. MM structural design: A three-layer Ag–Si–Ag stack in which the top layer is a periodic array of cross-shaped slots. Optimized parameters: array period p=4.6 μm, slot length L=1.4 μm, slot width w=0.9 μm, and layer thickness t=0.2 μm.

4.1.2. Results for the Transmissive NDIR–MM Sensor

The transmission and reflection spectra of the proposed MM filter are shown in Figure 4.2. Within the 3.6–4.8 μm band, the structure exhibits a distinct selective transmission peak at ≈ 4.26 μm, with transmittance ≈ 90%, while the reflection simultaneously drops to near zero (R ≈ 0).

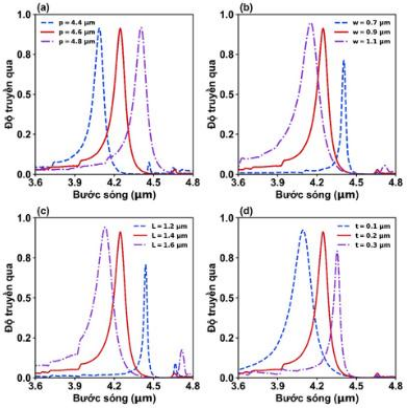

Figure 4.2. Transmission spectra of the MM filter under variations of geometric parameters: (a) effect of array period p; (b) effect of slot width w; (c) effect of cross-arm length L; (d) effect of dielectric/metal thickness t.

4.2. NDIR–MM Sensor in Reflective Configuration

4.2.1. Design of the Reflective NDIR–MM Sensor

The reflective configuration of the NDIR sensor integrated with MMs is illustrated in Figure 4.5(a). In this design, broadband infrared (IR) radiation from the source impinges on the MM mirror, which selectively reflects spectral components corresponding to specific wavelengths. The reflected radiation then passes through the gas sample chamber and reaches the IR detector. The proposed MM mirror consists of a two-layer structure, shown in Figure 4.5(b).

The bottom layer is a CaF_2 substrate with thickness z = 0.8 mm, The top layer comprises elliptical Si resonators with thickness h = 0.2 μm. Each ellipse has a major axis a = 2.2 μm and a minor axis b = 1.2 μm, oriented at $\theta = 20^0$ with respect to the y-axis. The structure is periodically arranged with period x = 4.2 μm and y = 2.9 μm.

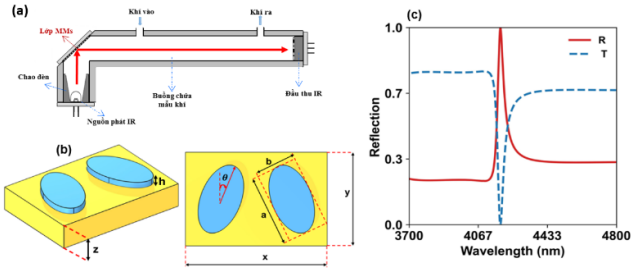

Figure 4.5. (a) Gas-sensor configuration; (b) MM mirror structure; (c) corresponding reflection spectrum.

4.2.2. Operation of the Reflective NDIR–MM Sensor

Figure 4.5(c) shows the reflection spectrum of the MM mirror, exhibiting a sharp reflection peak at 4260 nm with reflectance of ≈ 99.8 %. The nearly perfect reflection at the wavelength close to the CO_2 absorption band (~4200 nm) highlights the potential of MMs for high-sensitivity CO_2 gas sensing. This phenomenon of near-perfect reflection at 4260 nm can be explained theoretically by the conditions for total reflection, as discussed in [135, 136]. Perfect reflection occurs when the real part of the complex impedance approaches zero, satisfying the condition $\varepsilon'/\mu' < 0$. Moreover, a large imaginary component of refractive index (n'') is required to suppress evanescent tunneling and prevent light transmission through the thin film. To verify these conditions, the frequency-dependent effective parameters—impedance (Z), permittivity (ε), permeability (μ), and refractive index (n)—were extracted from the scattering parameters (S-parameters) using well-established analytical retrieval formulas [136-139]:

$$Z(\omega) = \sqrt{\frac{\left(1 + S_{11}(\omega)\right)^2 - S_{21}^2(\omega)}{\left(1 - S_{11}(\omega)\right)^2 - S_{21}^2(\omega)}}$$
$$n(\omega) = \frac{1}{kL}\arccos\left(\frac{1 - S_{11}^2 + S_{21}^2}{2S_{21}}\right) \quad (4.5)$$
$$\mu(\omega) = n(\omega)Z(\omega);\ \varepsilon(\omega) = \frac{n(\omega)}{Z(\omega)}$$

where k is the wavenumber and L is the unit-cell thickness.

4.2.3. Operating Mechanism of the MM Mirror

Figure 4.6(a) shows the real parts of the effective permittivity (ε′) and permeability (μ′), while Figure 4.6(b) presents the real part of impedance (Z′) and imaginary part of refractive index (n″). At the wavelength λ = 4260 nm, the real part of Z′ ≈ 0, the permittivity ε′ > 0, and the permeability μ′ < 0, while n″ reaches its maximum value..

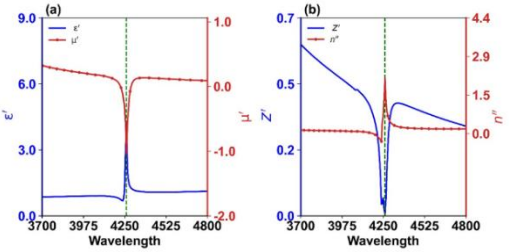

Figure 4.6. (a) Wavelength dependence of ε′, μ′; (b) variation of Z′ and n″.

Figure 4.7(a) displays the electric-field amplitude and field lines at λ = 4260 nm for two adjacent elliptical resonators. The electric field is strongly concentrated at the edges of the ellipses, with a maximum intensity of about 9.2×10^7 V/m. Figure 4.7(b) shows the magnetic-field amplitude and lines at the same wavelength, where the magnetic field is localized in the central region of the ellipses with a maximum of 3.0×10^5 A/m. The Figure 4.8 illustrates the influence of geometric parameters on the reflection spectrum. Varying the substrate length x from 4.0 μm to 4.4 μm produces a distinct red-shift of the resonance peak, indicating that an increase in lateral size enhances the resonant wavelength.

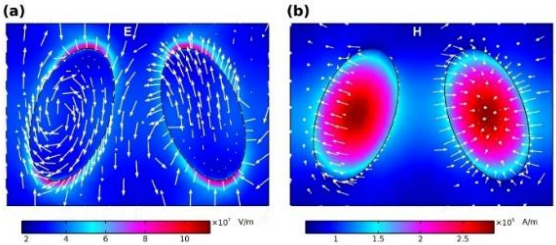

Figure 4.7. (a) Electric-field distribution; (b) magnetic-field distribution at λ = 4260 nm.

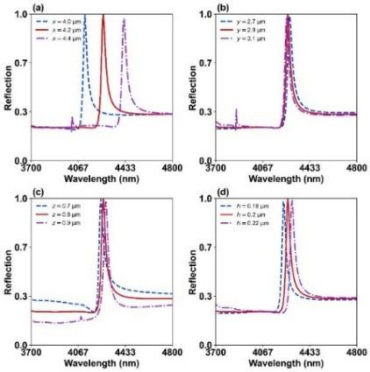

Figure 4.8. Dependence of reflection spectra on structural parameters: (a) substrate length, (b) substrate width, (c) substrate thickness, (d) resonator height.

4.2.4. Fabrication of the MM Infrared-Modulating Mirror

Figure 4.10 shows optical and scanning electron microscopy (SEM) images of three fabricated MM samples, denoted MMs_1, MMs_2, and MMs_3, each produced under different fabrication parameters.

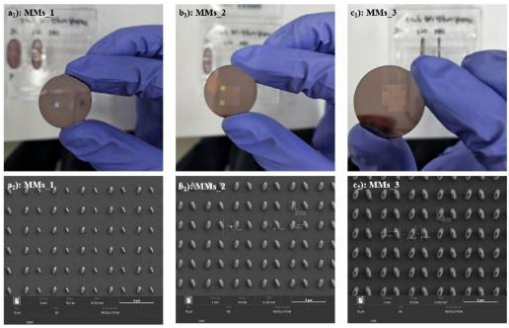

Figure 4.10. (a_1–c_1) Photographs of fabricated MM samples under three conditions; (a_2–c_2) corresponding SEM images.

Figure 4.11 presents the Fourier-Transform Infrared (FTIR) spectra (baseline-corrected) for the three MM samples. All spectra exhibit two main peaks—the first at 4228 nm and the second at 4275 nm. Although minor structural variations exist among the elliptical island arrays on the CaF_2 substrates, their spectral characteristics are remarkably consistent. The main FTIR peak for all samples is determined to be 4265 ± 95 nm.

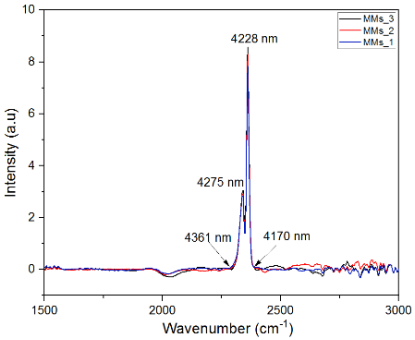

Figure 4.11. FTIR spectra of the three fabricated MM samples.

4.2.5. Fabrication of the Reflective NDIR Gas Sensor Integrated with MMs

Figure 4.12 shows the circuit schematic of the NDIR sensor. The IR source is driven by a 4 Hz square-wave voltage, with frequency controlled by a quartz-oscillator circuit. The output signal from the dual-channel IR detector—comprising a reference channel and a gas-sensitive channel—is typically collected via a MOSFET-based amplifier

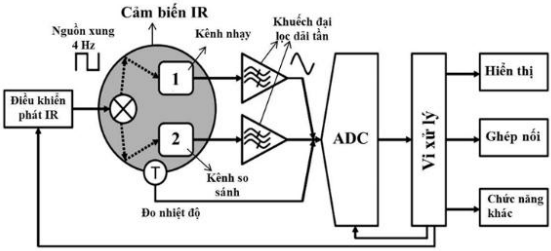

Figure 4.12. Schematic circuit diagram of the NDIR gas sensor.

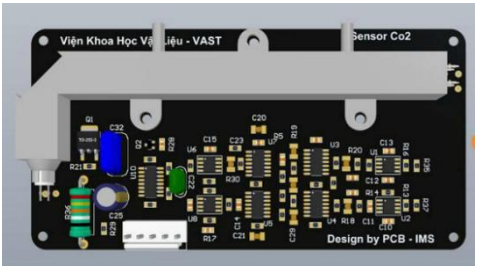

Figure 4.15. Printed-circuit-board (PCB) layout for the MM-integrated NDIR sensor.

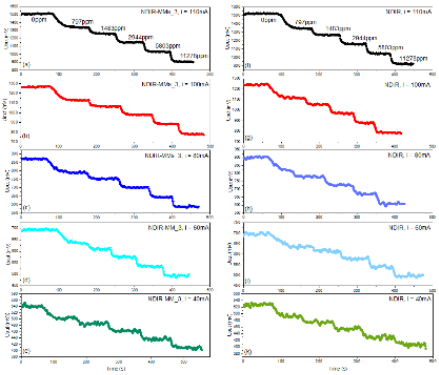

Figure 4.17. (a) Diagram of the gas-mixing system; (b) corresponding experimental setup.

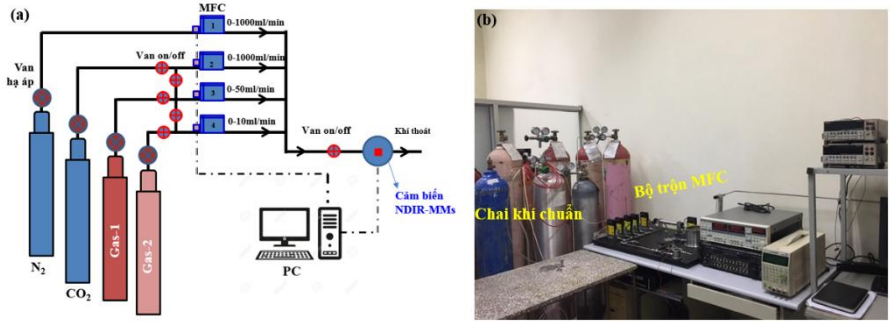

Figure 4.20. Output voltage of the sensitive channel for conventional NDIR and MM-integrated NDIR sensors as a function of IR-lamp driving current (40–110 mA).

4.3. Summary of Chapter 4

The use of MM-based infrared modulators as substitutes for conventional optical filters simplifies sensor design, reduces energy consumption, and enables direct integration into NDIR systems. In the reflective configuration, the fabricated MM layer was successfully implemented and tested in an NDIR CO_2 sensor, yielding promising experimental results. Beyond CO_2 detection, the same design principle can be extended to sense other gases with different absorption wavelengths by adjusting the geometric parameters of the MM structure.

GENERAL CONCLUSION

This dissertation has conducted comprehensive research and achieved significant results on metamaterials (MMs) for integration into non-dispersive infrared (NDIR) gas sensors, as follows:

(I) Transmission configuration:

MMs were integrated onto the surface of a micro-heater to form a narrowband infrared (IR) emission source tailored for CO_2 detection. The unit cell, consisting of circular resonators and cavity structures, generated two strong magnetic resonances at 3960 nm and 4197 nm with high absorption efficiencies of 96.3% and 94.1%, respectively. When integrated onto a zigzag-type micro-heater, the IR-MMs emitter achieved an approximately 35% reduction in power consumption compared to a conventional blackbody source, with emission intensities of 1.75×10^9 and 1.8×10^9 $W\cdot sr^{-1}\cdot m^{-3}$. This design demonstrates enhanced spectral selectivity and extended operational lifetime for NDIR applications.

Additionally, a cross-shaped slot MMs structure was simulated as a narrowband optical filter tuned to the CO_2 absorption wavelength (4.26 μm), showing >90% transmittance with a full width at half maximum (FWHM) of 180 nm. Theoretical analysis indicated a signal attenuation of only 3.8% at 573 K, confirming its potential for selective CO_2 detection with high energy efficiency.

(II) Reflection configuration:

An NDIR sensor integrated with a reflective MMs layer based on elliptical Si resonators on a CaF_2 substrate (z = 0.8 mm, x = 4.2 μm, y = 2.9 μm, $\theta = 20^0$) was designed and fabricated. Experimental results showed that the MMs layer significantly enhanced the sensor's sensitivity: sensitivity increased from 0.20134 to 0.20991 / 1 ppm, the limit of detection (LoD) decreased from 0.1569 ppm to 0.126 ppm, and the standard deviation (SD) reduced from 19.87 ppm to 15.65 ppm over the 0–10,000 ppm CO_2 concentration range.

In summary, the dissertation demonstrates that incorporating metamaterials into NDIR sensors substantially improves their efficiency, spectral selectivity, and detection sensitivity, offering a promising pathway toward compact, energy-efficient CO_2 sensing systems.

LIST OF PUBLICATIONS RELATED TO THE DISSERTATION

1. Trinh My Anh, Dang Le Gia Han, Mai Ngoc Linh, **Pham Duy Tan**, Bui Xuan Khuyen, Ho Truong Giang, *"Nghiên cứu chế tạo cảm biến NDIR đo khí CO_2 dải nồng độ thấp để áp dụng cho điều hòa không khí trong nhà giảm tác động xấu đến sức khỏe con người"*, Journal of Military Science & Technology **77**, 120-127 (2022).

2. Pham Duy Tan, Dinh Ngoc Dung, Nguyen Van Ngoc, Vu Thi Hong Hanh, Soulima Khamsadeth, Bui Son Tung, Bui Xuan Khuyen, Ho Truong Giang, Vu Dinh Lam, *"Nghiên cứu mô phỏng vật liệu biến hóa phát xạ hồng ngoại ứng dụng cho cảm biến khí CO_2"*, Proceedings of the 12th National Conference on Solid State Physics and Materials Science (SPMS 2021), August 13–15, Can Tho City, Vietnam, Volume 2, 640-644 (2022), ISBN: 978-604-316-838-9.

3. Pham Duy Tan, Duong Thi Ha, Bui Son Tung, Bui Xuan Khuyen, Do Thuy Chi, Vu Dinh Lam, Liangyao Chen, Haiyu Zheng and Youngpak Lee, *"Recoverable Broadband Absorption Based on Ultra-Flexible Meta-Surfaces"*, Crystals **12**, 1817 (2022).

4. Pham Duy Tan, Dang Tuan Dat, Pham Quang Ngan, Pham Dinh Tuan, Nguyen Ngoc Khai, Bui Xuan Khuyen, Ho Truong Giang, Vu Dinh Lam, *"Tích hợp ESP32 vào bo mạch cho cảm biến NDIR đo khí CO_2 để ứng dụng nền tảng IoT trong nuôi trồng nấm ăn"*, Conference on Solid State Physics and Materials Science (SPMS 2023), November 5–7, Ho Chi Minh City, Vietnam, Volume 1, 315-319 (2023), ISBN: 978-604-471-702-9.

5. Bui Xuan Khuyen, Nguyen Van Ngoc, Dinh Ngoc Dung, Nguyen Phon Hai, Nguyen Thanh Tung, Bui Son Tung, Vu Dinh Lam, Ho Truong Giang, **Pham Duy Tan**, Liangyao Chen, Haiyu Zheng, and YoungPak Lee, *"Dual-band infrared metamaterial perfect absorber for narrow-band thermal emitters"*, Journal of Physics D: Applied Physics **57** (28), 285501 (2024).

6. Bui Xuan Khuyen, **Pham Duy Tan**, Bui Son Tung, Nguyen Phon Hai, Pham Dinh Tuan, Do Xuan Phong, Do Khanh Tung, Nguyen Hai Anh, Ho Truong Giang, Nguyen Phuc Vinh, Nguyen Thanh Tung, Vu Dinh Lam, Liangyao Chen, YoungPak Lee, *"Numerical Optimization of Metamaterial-Enhanced Infrared Emitters for Ultra-Low Power Consumption"*, *Photonics* ***12*** (6), 583 (2025).